Axial crushing of aluminum extrusions filled with PET foam and GFRP. An experimental investigation.

M. Costas[a,*], D. Morin[b], M. Langseth[b], L. Romera[a], J. Díaz[a]

[a]*Structural Mechanics Group, School of Civil Engineering. University of A Coruña. Campus de Elviña, 15071, A Coruña, Spain*

[b]*Structural Impact Laboratory (SIMLab) and Centre for Advanced Structural Analysis (CASA) - Centre for Research-based Innovation. Department of Structural Engineering, Norwegian University of Science and Technology (NTNU), NO-7491 Trondheim, Norway*

Abstract

This research work investigated the axial crushing behavior of a circular aluminum extrusion in alloy AA6063-T5 filled with polymeric foam and a glass-fiber structure. The components were experimentally tested under quasi-static and impact loading conditions supported by a material testing campaign. Energy absorption, crush force efficiency and specific energy absorption were experimentally measured in order to assess the performance of a design proposal. Besides, the interaction effects between the different materials has been analyzed in depth and compared to the results for aluminum foam filled extrusions available in the literature. The confinement effect of the foam on the glass fiber plates has been found to have a very remarkable contribution to the energy absorption levels of the component, whereas a negligible foam-extrusion interaction was observed due to the gaps in the initial geometry of the specimen. The investigated component show an overall good performance, specially in terms of crush force efficiency. However, the specific energy absorption of the component was reduced by approximately 10 % compared to the aluminum extrusion alone.

Keywords: Crashworthiness, aluminum extrusion, glass-fiber, polymeric foam, experimental testing

1. Introduction

Aluminum and structural foams are materials which have gained great popularity in the automotive industry over the past 10-15 years. The first offers a very remarkable weight saving compared to steel and the latter allows to improve the stiffness of specific areas like

*Corresponding author. Tel: +34 881 01 6101

Email addresses: miguel.costas@udc.es (M. Costas), david.morin@ntnu.no (D. Morin), magnus.langseth@ntnu.no (M. Langseth), lromera@udc.es (L. Romera), jdiaz@udc.es (J. Díaz)

the top parts of the A and B pillars, increasing their bending stiffness [1, 2]. One particular field in which both materials are particularly useful is in crash boxes of vehicles, since aluminum crash boxes are able to absorb a high amount of energy with a reduced weight. Foams are usually regarded as a filling for these members.

The first investigations on the energy absorption of thin-walled metal tubes date from the 1960's with the works by J. M. Alexander [3], who obtained also a theoretical expression for the mean crushing force of circular tubes. This expression was later improved in the works by Wierzbicki and Abramowicz [4, 5] and extended to square sections. Additional experimental testing campaigns carried out in the 1980s and 1990s [6–9] validated the quality of the theoretical predictions.

Regarding the use of foams as a filling for the crash-absorbing parts, the first studies date from the late 1980s by Reid et al. [10, 11]. Later comprehensive investigations by Hanssen et al. in the 2000's must be highlighted as well. In these, the authors studied experimentally the crashworthiness of aluminum extrusions filled with aluminum foam, and proposed a design formula which also takes into account the strong interaction effect between the foam and the thin walls of the extrusion. This effect had a very noticeable contribution to the energy absorption levels of their designs. Square [12] and circular [13] foam-filled sections were studied, and numerical models were calibrated by Santosa et al. to support this research campaign [14]. A parallel experimental and numerical study on the axial crushing of steel members filled with high-density aluminum foam was carried out by Seizberger et al. in 2000 [15]. Finally, Reyes et al. investigated the oblique loading of foam-filled aluminum extrusions [16]. The main conclusion of these works was that the absorbed energy can be increased with the foam filler but the increase in weight generally decreases the efficiency of the filled tube when compared to the empty extrusion.

Polymeric foams are a good alternative to the aluminum foam as an inner reinforcement for crash boxes. In 1986, the works by Reid et al. [10, 11] firstly explored this possibility with polyurethane foams of different densities, and stating some simple theoretical models for the interaction effect. A literature review shows that a considerable effort has been made since then in the mechanical characterization of these materials at different strain rates [17–20], but only a reduced number of studies can be found on its application to crash boxes. These studies included foam-filled composite profiles ([21, 22]) and the work by Costas et al. [23] where a polyethylene terephthalate (PET) foam considered as an inner reinforcement for steel tubes showed good results. The design proposed in the present work arises from the good performance of PET foam and glass-fiber filled steel tubes

investigated in [23].

The specimens studied in the present work include also an additional inner reinforcement of fiberglass sheets. A large number of works are present in the literature also for fiber-reinforced metal tubes, most of them focusing on tubes reinforced with externally bonded fibers. This offers the possibility of increasing the crushing force levels with a high-strength, lightweight material. As for the empty and foam-filled extrusions, early theoretical expressions for the mean crushing load of externally reinforced metal tubes can be found in the works by Hanefi and Wierzbicki [24]. Later work by Song et al. [25] extended the formulation to impact loads by accounting for the strain-rate sensitivity of metals. References on the assessment of different design proposals can be found on either carbon [26, 27] or glass-fiber reinforced polymers [28, 29]. The inner reinforcement of metal tubes with composite structures is more uncommon, but some recent references can be found in [30, 31].

In [23], the authors claimed that steel tubes internally reinforced with a glass fiber reinforced polyamide (GFRP) structure or a PET-based foam increased their specific energy absorption compared to the steel tubes alone. This enhancement was mainly due to the contribution of the reinforcement itself to the energy absorption and the well-known interaction between the foam and metal parts. However, it was observed that the efficiency of the design with an inner GFRP structural reinforcement could be significantly enhanced with some kind of constraining or confinement system which prevented the GFRP parts to fall apart after incipient fracture. With this motivation, the present work combined both materials (PET foam and GFRP). These were enclosed in an aluminum circular extrusion without bonding, and the interaction effect has been analyzed.

The crash box shown in Figure 1a consists of an AA6063-T5 aluminum extrusion internally reinforced with a structure made of a glass-fiber reinforced polyamide. The gaps between both parts are then partially filled with polymeric foam prisms. To simplify the manufacturing process, these foam prisms were cut in triangular sections and inserted in the structure, so the contact is not closed between foam and aluminum. The total length of the component was 350 mm and its mass was equal to 1736 g. The length of the foam prisms was equal to the total length of the component, and the length of the GFRP plates was reduced to 348 mm to avoid an overlapping of the initial peak forces of the extrusion and the GFRP.

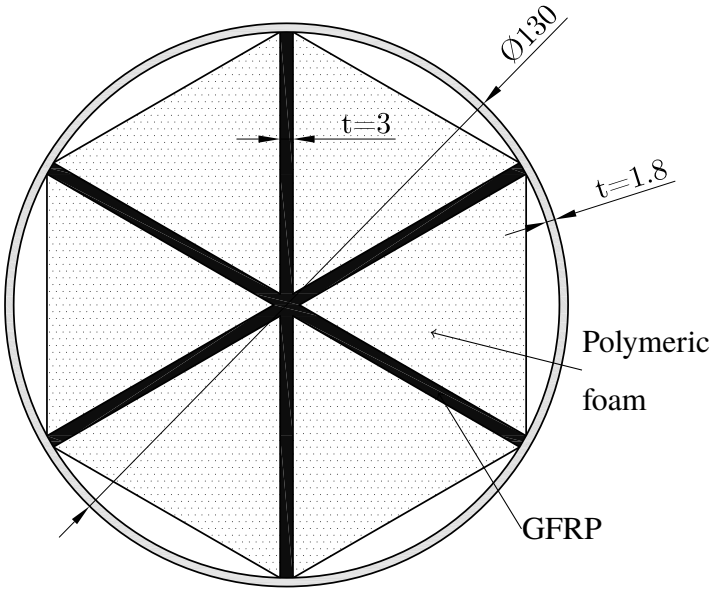

(a) Cross-section of the crash box.

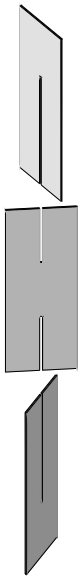

(b) GFRP assembly.

Figure 1: Cross-section of the proposed crash box made of aluminum (gray), polymeric foam (dotted) and GFRP plates (black) and assembly scheme. Dimensions in millimeters.

2. Material behavior

In order to help to understand the performance of the proposed design, a test campaign was planned to obtain the mechanical properties of the selected materials. These tests and their results are described next.

2.1. AA6063-T5 aluminum alloy extrusion

Since the material properties of metals have a strong dependency on the industrial production process, material specimens extracted from the same extruded circular hollow aluminum sections employed for the crash boxes were tested. These extractions were made so that their longitudinal axis was aligned with the extrusion direction of the tubes, which inevitably leads to a certain curvature of the specimens. The detailed geometry of the tensile specimens is shown in Figure 2.

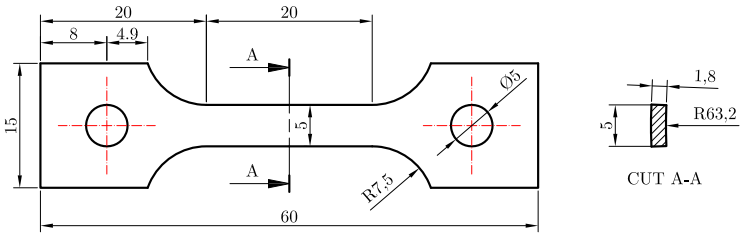

Figure 2: Dimensions of the AA6063-T5 tensile specimens extracted from the tubes in their longitudinal direction, in millimeters.

Tensile tests have been performed on three specimens at a constant rate of 1 mm/min and true stress-strain curves were obtained, provided in Figure 3. Strain values were measured with an extensometer, so they are valid up to diffuse necking only.

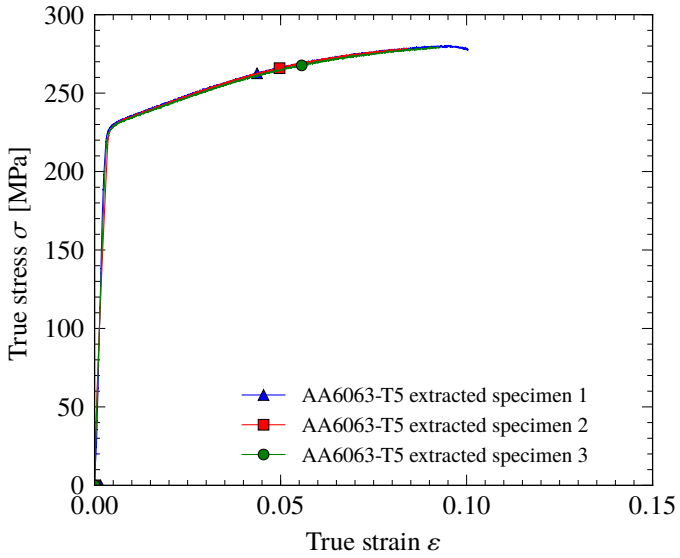

Figure 3: AA6063-T5 extrusion true stress-strain curves obtained from experimental tensile tests on specimens extracted from circular hollow extrusion.

The high yield strength and reduced hardening shown in Figure 3 are common for tempers T5 and T6 in the 6xxx series. Some useful mechanical properties have been obtained from these tests and included in Table 1. Negligible strain rate sensitivity was expected, as usually happens with 6xxx alloys [32, 33].

Property	Value
Density [t/m^3]	2.56
Young's modulus [GPa]	53.85
Poisson ratio	0.33
Initial yield stress [MPa]	225.00

Table 1: Material properties of aluminum alloy AA6063-T5 in circular hollow extrusion.

2.2. Glass-fiber reinforced polyamide

The first reinforcement part was made of a glass-fiber reinforced polyamide with commercial name Ultramid A3WG10 BK00564 (BASF). This material consists of a 50% glass fiber reinforced PA66 in which very short fibers with random orientations are chopped

into a polyamide matrix. The parts were built by injecting 3-millimeter thick plates, cutting them and assembling the three elements required for each tube in the way shown in Figure 1b. Some tensile tests on plane specimens at different strain rates were conducted to get some information about its behavior, even though higher strain rates were reached in the component impact tests. The dimensions of the plane specimens are plotted in Figure 4.

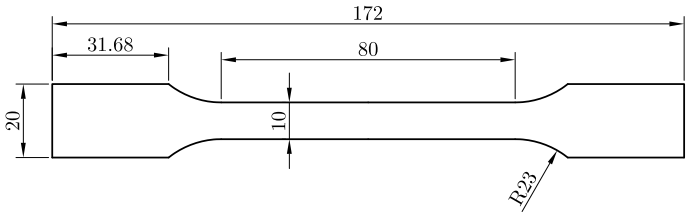

Figure 4: Dimensions of the GFRP plane tensile specimens, in millimeters.

The material was tested in tension up to failure at strain rates of 3.25×10^{-5}, 3.25×10^{-4} and 8.12×10^{-3} s^{-1}, which correspond to test speeds of 0.2, 2 and 50 mm/min, respectively. Three repetitions were made for each speed, and representative curves are plotted in Figure 5.

In view of the curves, the material exhibits a certain degree of strain rate sensitivity for the $\dot{\varepsilon}$ levels tested. A value of 15.48 GPa is obtained for the Young's modulus, which indicates a relatively stiff thermoplastic material. Its density (1.55 t/m^3) and Poisson's ratio (0.40) are available in [34], together with the theoretical elastic modulus and other mechanical properties.

It can also be observed that the failure strain tends to rise with higher strain rates: 2.14% at $3.25 \times 10^{-5} s^{-1}$, 2.38% at $3.25 \times 10^{-4} s^{-1}$ and 2.54% at $8.12 \times 10^{-3} s^{-1}$.

2.3. PET-based polymeric foam

The second element of the reinforcement consists of six prisms of a PET-based, closed-cell foam with commercial name ArmaFORM PET/W AC 135. Six triangular prisms are inserted between the glass fiber plates and the extruded tube, as shown in Figure 1a.

Given that this material is manufactured through an extrusion process, some anisotropy in the mechanical properties can be expected. Therefore, the material parameters were obtained in the load direction of the crash box, which is orthogonal to the direction in which the foam was extruded during its manufacture process. Meeting the requirements of ISO 844:2014 [35], specimens of $50 \times 50 \times 30$ mm were extracted and loaded in uniaxial compression at different rates along the 30 mm direction, which is orthogonal to the extrusion orientation. Additionally, this material was tested at an elevated strain rate

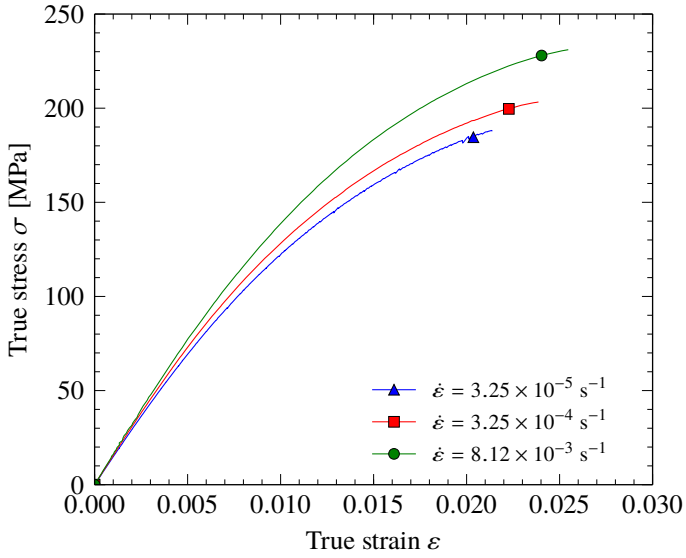

Figure 5: True stress-strain curves obtained from experimental uniaxial tests at different strain rates from smooth tensile specimens of Ultramid A3WG10 BK00564

using a drop tower in which a mass of 8 kg was dropped at 6.78 m/s on specimens with dimensions $50 \times 50 \times 40$ mm, cut in the same direction as the ones for the quasi-static compression tests.

True stress-strain curves were computed taking into consideration the compressibility of the material, as follows:

$$\sigma = s \exp\left(-2\nu^p \varepsilon_1\right), \tag{1}$$

where σ is the true stress, s is the engineering stress, ν^p is the plastic Poisson ratio and ε_1 are the axial true strains. An additional assumption was made when it comes to obtaining the plastic Poisson's ratio, originally defined for isotropic materials as the ratio of the transverse plastic strains to the plastic strain in the load direction:

$$\nu^p = \frac{\varepsilon^p_{2,3}}{\varepsilon^p_1}. \tag{2}$$

Considering the anisotropy of the material ($\varepsilon^p_2 \neq \varepsilon^p_3$) the mean value of both transverse directions was used to obtain the transverse plastic strain. According to this, a value of $\nu^p = 0.089$ is derived from the uniaxial compression tests.

Table 2 contains a summary of the mechanical properties of the PET foam in the orientation orthogonal to the extrusion direction, and the stress-strain curves for three different loading rates are plotted in Figure 6. The continuous line for 6.78 m/s is an average of the original signal (dashed line) so that the noise arising from stress waves traveling along the load cell can be removed. Some strain rate sensitivity was observed.

Property	Value at 6 mm/min
Density [t/m^3]	0.135
Young's modulus [MPa]	20.41
Elastic Poisson ratio	0.10
Initial yield stress [kPa]	770.00
Plastic Poisson's ratio	0.09

Table 2: Material properties and model parameters of ArmaFORM PET/W AC 135 PET-based foam in the direction orthogonal to extrusion

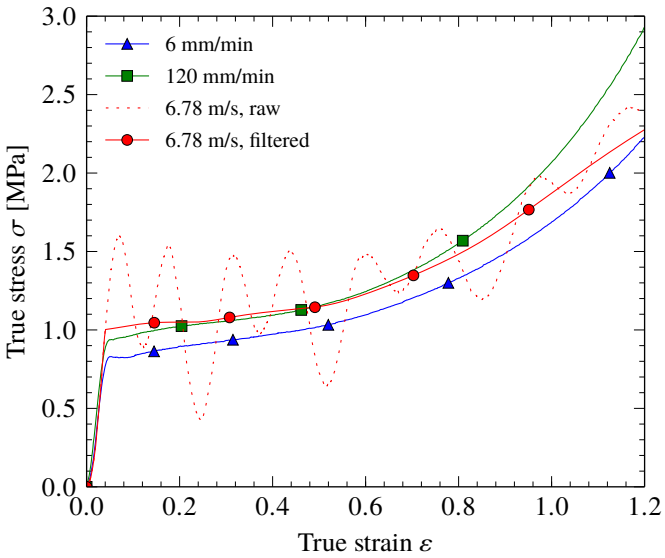

Figure 6: True stress-strain curves from uniaxial compression tests at different loading rates for Armaform PET/W AC 135 PET-based foam in the direction orthogonal to the extrusion direction.

3. Component testing program

3.1. Quasi-static compression tests

Low-speed compression tests were carried out on the components to assess their quasi-static behavior. An INSTRON 1332 universal test machine was employed for this task. Components were axially compressed at a constant rate of 50 mm/min until bottoming out of the part, i.e. approximately 200-250 mm. Three parallel component tests were carried out and named C1, C2 and C3. Additionally, for comparative purposes, an empty circular extrusion (C0), a glass-fiber reinforced extrusion (CG) and a foam-filled extrusion (CF) were tested as well. Table 3 contains a summary of the tested components in the quasi-static campaign.

All specimens were triggered at their impacted ends by bending inwards the generatrix edge of the aluminum extrusion about 2 mm, forcing the progressive collapse to start with a stable concertina mode. For all components except C0, triggering was only possible in those regions which are not in initial contact with the glass-fiber structure or the foam (see Figure 1a). For the sake of consistency, the same triggering pattern in specimen C0 was used even though its entire edge could be bent inwards. Minor geometrical imperfections were also detected in the cross-section of the extrusion consisting of a deformation about 1 mm in the circular geometry, and the triggering helped also to avoid undesired collapse modes caused by this fact.

3.2. Dynamic impact tests

Crash boxes should behave in a similar, predictable way independently of the impact speed. In order to verify this point, dynamic impact tests were carried out on the chosen design. Components were tested at a high rate using a large pendulum accelerator, Figure 7. The reader is referred to [36] for a detailed description of the pendulum accelerator at SIMLab, but a brief description is provided next. The test rig consists of a hydraulically-actuated rotational arm which accelerates a trolley with a mass of 1500 kg to a certain velocity. The trolley was equipped with a 500 kN load cell in order to obtain forces, displacements, velocities and accelerations. Displacement measurements were also checked with a high-speed camera which recorded the impact behavior at a frame rate of 16000 frames per second. The differences between both measurements were negligible. Initial impact velocities were checked with a photocell, which provided an estimated error of a 1.3% on the preset speed of 10 m/s. The last 50 mm of the specimens were clamped and screwed to a massive concrete reaction wall (150 000 tonnes), which gives a

free deformation length of 300 mm. For safety reasons, two buffers had to be placed at both sides of the specimen to stop the trolley safely and to avoid extreme force values in the load cell due to the bottoming-out of the specimens. This caused that the obtained force-displacement curves were only valid before the contact between the trolley and the buffers, which in this case occurred after 185 mm of axial crushing. A photograph of the clamped component and the two safety buffers is provided in Figure 8. Two components were tested at 10 m/s under the described impact conditions, labeled D1 and D2 (see test matrix in Table 3).

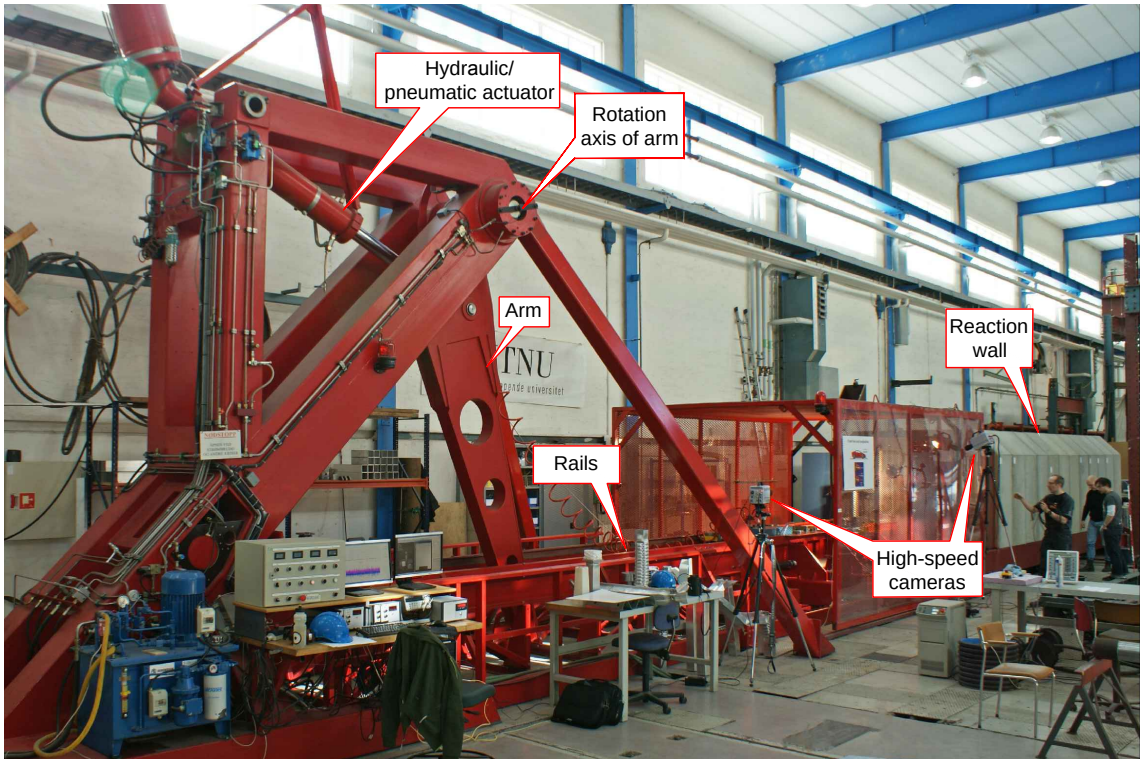

Figure 7: The «kicking machine» or pendulum accelerator at SIMLab facilities. Image taken from [37], used with permission.

4. Results and discussion

4.1. Quasi-static compression tests

The force-displacement curves obtained from the quasi-static axial crushing tests are shown in Figure 9 for an empty tube and for tubes with reinforcement. The current average crushing force is also provided in Figure 10, obtained as

$$F_{\text{avg}} = \frac{1}{\delta} \int F \mathrm{d}\delta. \tag{3}$$

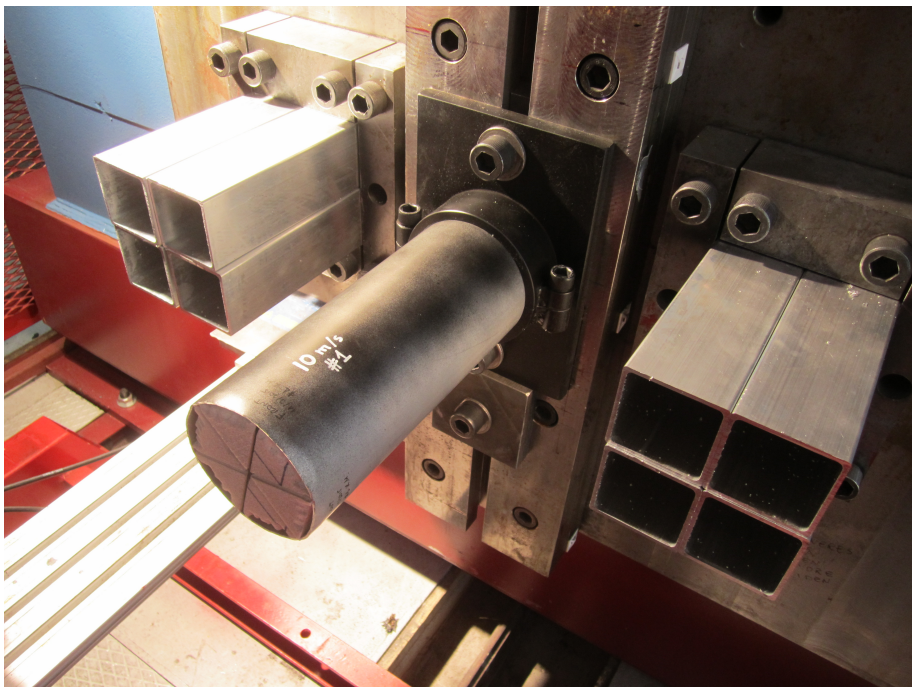

Figure 8: Impact test set-up: component (center) and safety buffers (sides). The component is airbrushed with black paint to avoid reflections in the images captured by the top camera.

As additional information, Figure 11 contains some sequential pictures of the tests where the different collapse modes can be observed.

It is interesting to point out the different modes developed by the component depending on its inner reinforcement:

- The empty tube (C0) developed a concertina-like collapse at the beginning (due to triggering) which evolved into a three-lobe diamond mode. Although the latter is theoretically more efficient for energy absorption purposes, it is also true that larger strains are reached in the vertices and therefore fracture can be present. This is specially threatening in aluminum alloys with temper T5 or T6, which are less ductile than, for example, T4. It was indeed observed some incipient fracture in this specimen in the diamond lobes. In fact, a first fracture can be easily observed in the transition between the two modes in the force-displacement curves, at a crushing distance of 90 mm approximately, Figure 9. Besides, the lobe wavelengths for the diamond mode are larger than the ones for the concertina mode, thus a minor number of lobes can be developed with a diamond-like collapse. This specimen showed six concertina lobes (three inwards and three outwards) and four alternate triangles up to a crushing length of 250 mm. This relatively high number of lobes is due to the reduced hardening shown by the T5 temper (Figure 3), which concentrates the yielded regions and therefore the lobe lengths are reduced. A picture of the axially

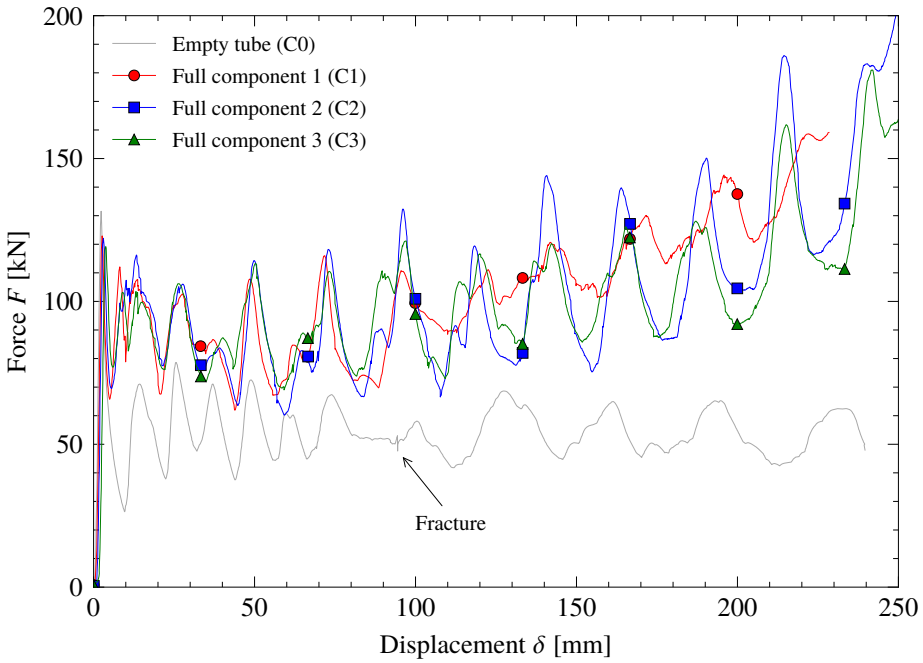

Figure 9: Force-displacement curves resulting from the quasi-static axial crushing of different configurations

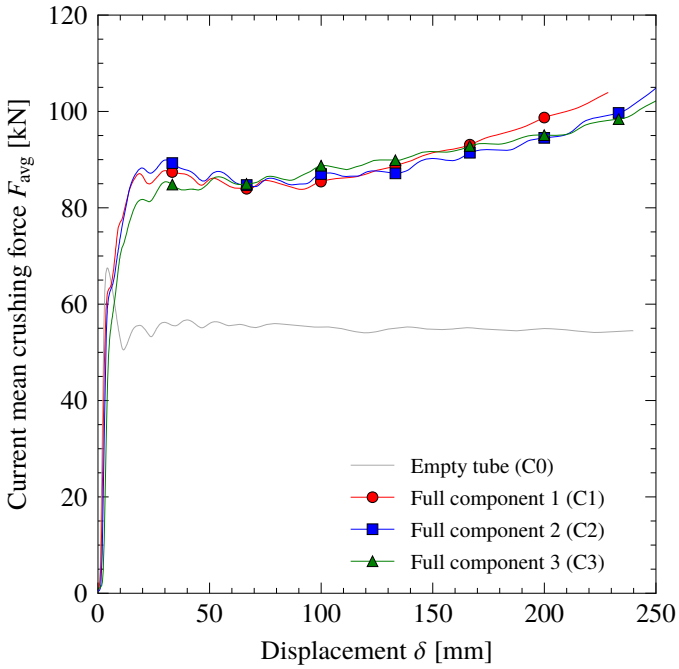

Figure 10: Current mean crushing force of the quasi-static compression tests for components C0, C1, C2 and C3.

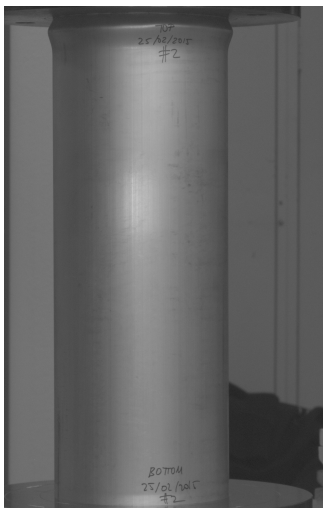

(a) $\delta = 4.7\,\text{mm}$

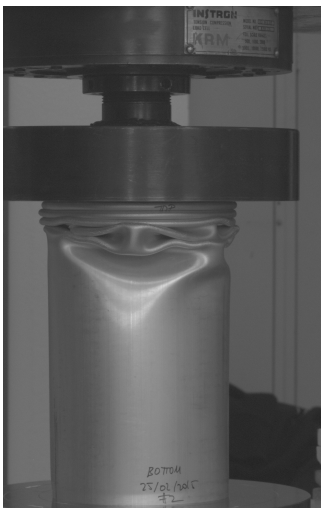

(b) $\delta = 137.1\,\text{mm}$

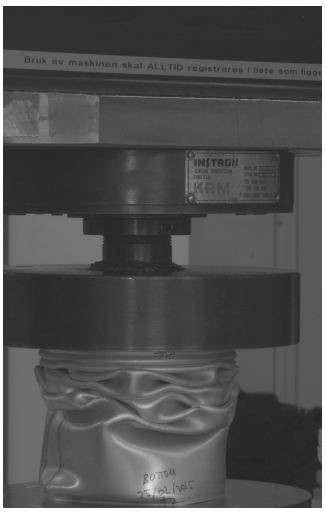

(c) $\delta = 239.0\,\text{mm}$

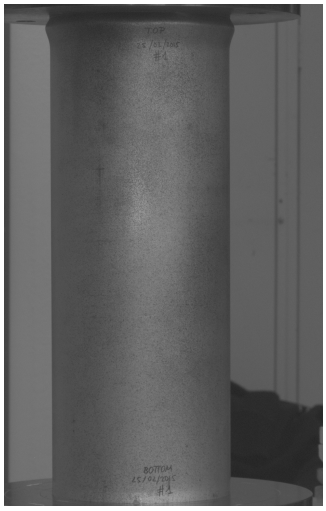

(d) $\delta = 5.0\,\text{mm}$

(e) $\delta = 137.4\,\text{mm}$

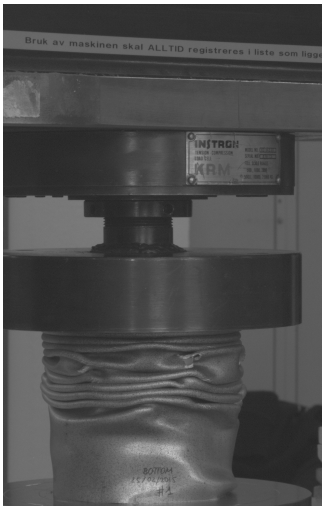

(f) $\delta = 228.0\,\text{mm}$

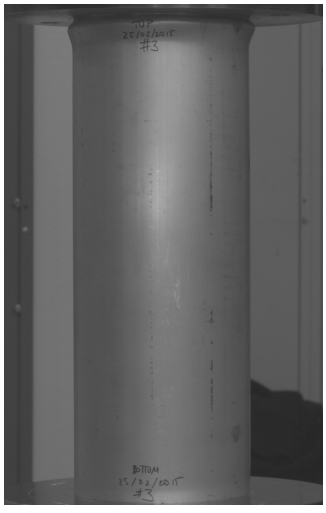

(g) $\delta = 5.0\,\text{mm}$

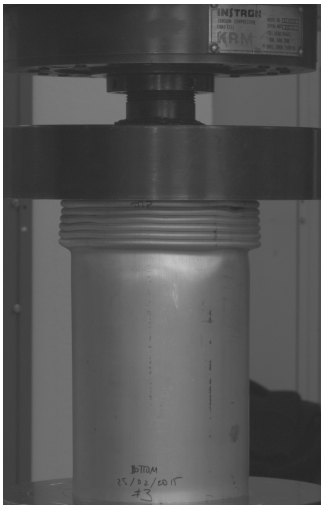

(h) $\delta = 137.4\,\text{mm}$

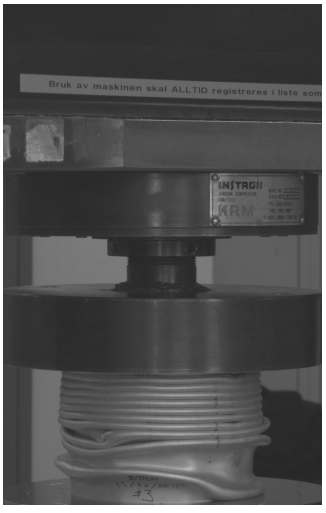

(i) $\delta = 255.7\,\text{mm}$

Figure 11: Quasi-static compression tests: progressive collapse of specimen C0 (a to c), and components C1 (d to f) and C2 (g to i). The collapse mode of the component C3 was omitted here for brevity, as it was identical to C2.

Component label	Characteristics	Test speed
C0	AA6063-T5 extrusion	Quasi-static
CG	AA6063-T5 extrusion + GFRP structure	Quasi-static
CF	AA6063-T5 extrusion + PET-foam prisms	Quasi-static
C1, C2 and C3 (repetitions)	Full component: AA6063-T5 extrusion + GFRP structure + PET-foam prisms	Quasi-static
D1 and D2 (repetition)	Full component: AA6063-T5 extrusion + GFRP structure + PET-foam prisms	Impact at 10 m/s

Table 3: Summary of the testing campaign: labels and descriptions of the tested designs

crushed specimen C0 is presented in Figure 12a.

- Specimen CG exhibited the same pattern as C0: six concertina folds (three inwards, three outwards) and a series of diamond lobes. These are slightly more irregular due to the presence of the glass fiber plates inside the structure. Relatively large fragments of the plates were found after the test, so the energy absorption of this design is not exploited at its best. The force-displacement curve for this specimen is analyzed in Section 4.4 (Figure 16a), and a picture of the crushed specimen is offered in Figure 12b.

- Specimen CF developed a transition mode very similar to the one observed in specimen C0, with four concertina lobes (two inwards, two outwards) followed by a series of diamond-like lobes. Also, only very minor fracture initiations were observed in some corners of the diamond lobes. The similarities between C0 and CF are explained by the presence of gaps between the foam prisms and the outer extrusion in the undeformed configuration, which prevents any interaction of the foam with the extrusion. The reader is referred to Figure 16a for the force-displacement curve of CF and Figure 12c for a picture of the crushed specimen.

- Regarding the full components, component C1 showed also a combined collapse

mode (concertina to 3-lobe diamond) with some crack initiations in the triangular lobes, which are perceptible in Figures 11e and 11f. However, components C2 and C3 developed a very stable concertina collapse mode with 19 folds developed at a crushing distance of 225 mm, and the differences between these two were minimum. Crushed component C3 is depicted in Figure 12d. Nevertheless, even though C1 collapsed in a mixed mode, the average force levels for the three full components were very similar (Figure 9).

4.2. Crashworthiness assessment

A well-known terminology has been used to evaluate the structural crashworthiness of the tested components. These are:

Absorbed energy (E_a) The energy absorbed during crushing can be obtained as the area under the load-displacement curve:

$$E_a = \int_0^{\delta_{\max}} F(\delta)\,\mathrm{d}\delta\,, \tag{4}$$

where $\delta_{\max}$ is the total axial crushing distance and $F(\delta)$ the value of the crushing force.

Specific Energy Absorption (*SEA*) It is defined as the ratio between the absorbed energy and the mass of the specimen (m):

$$SEA = \frac{E_a}{m}. \tag{5}$$

Mean crushing load (P_m) The mean of the values of the crushing force. It can be obtained as the ratio of the absorbed energy to the total displacement of the specimen's head or crushing length ($\delta_{\max}$):

$$P_m = \frac{E_a}{\delta_{\max}}. \tag{6}$$

Crush force efficiency (CFE) The ratio between the mean load (P_m) and the initial peak load (P_{peak}). This crush force ratio should be as high as possible, in order to reduce

(a) Specimen C0

(b) Specimen CG

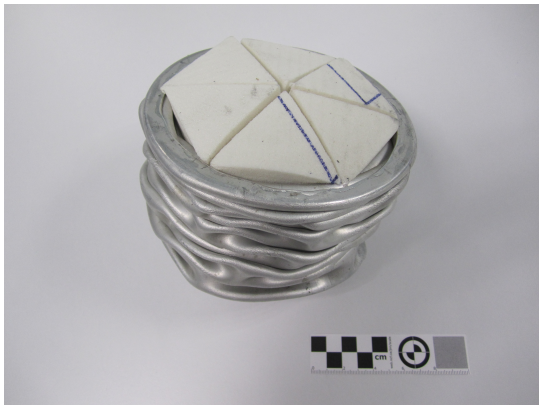

(c) Specimen CF

(d) Component C3

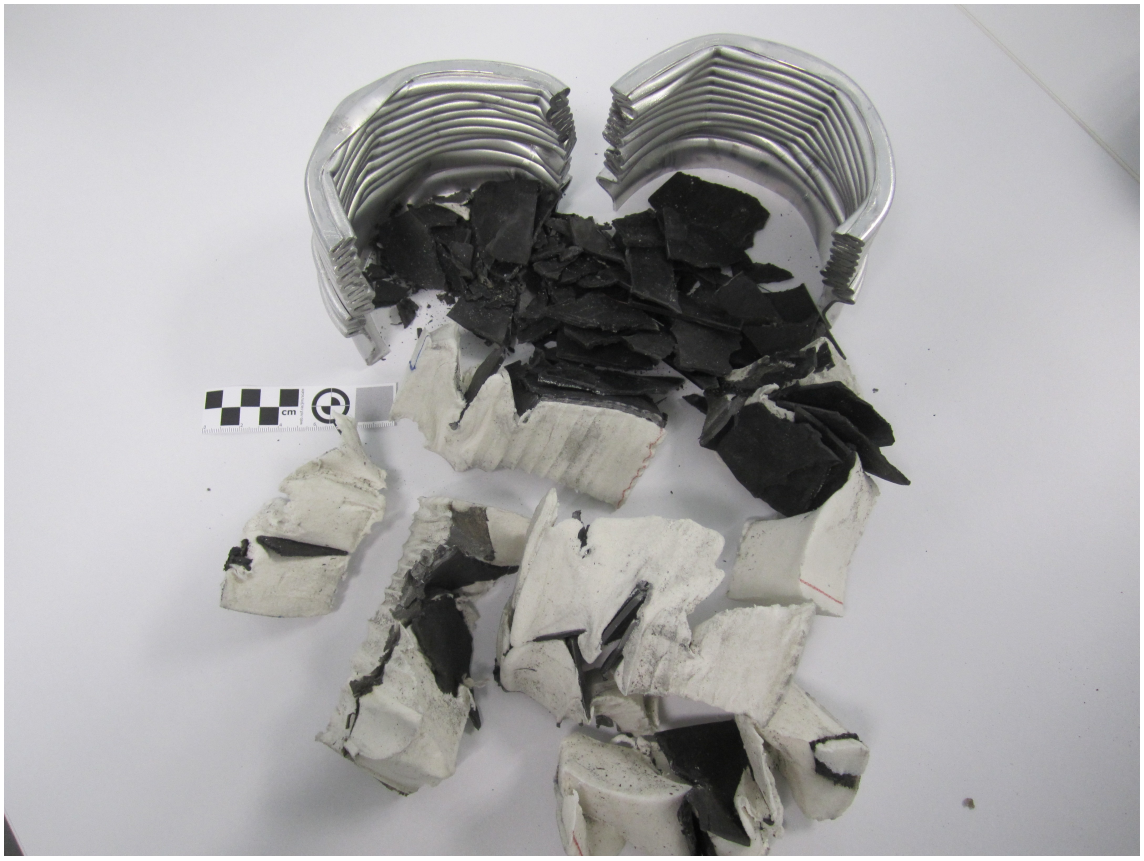

(e) Component C2 cut and unassembled for analysis

Figure 12: Specimens C0, CG, CF and component C3 after quasi-static axial crushing

the eventual accelerations peaks suffered by the occupants during a crash and the strong variations in the forces transmitted to other structural members:

$$CFE = \frac{P_m}{P_{\text{peak}}}. \tag{7}$$

The previous crashworthiness indicators have been obtained for a crushing length of 228 mm (65%) for the proposed design and the empty extrusion. A very remarkable increase in the absorbed energy is achieved, even though the specific energy absorption of the design is slightly reduced compared to the aluminum extrusion alone. Besides, the crush force efficiency is strongly enhanced as well, since there is almost no difference between the initial peak load and the mean load. The differences in the initial peak loads for identical components (C1, C2, C3) lie in the minor differences when triggering the components manually. These results can probably be improved with a larger crushing distance since no clear bottoming-up was reached. All results are listed in Table 4, including the developed collapse modes: C (concertina), D3 (3-lobe diamond).

	Collapse mode	Mass [g]	P_{peak} [kN]	P_m [kN]	CFE	E_a [kJ]	SEA [kJ/kg]
Specimen C0	C→D3	738	131.56	53.84	0.41	12.30	16.66
Component C1	C→D3	1737	122.92	103.19	0.84	23.57	13.57
Component C2	C	1737	122.12	98.70	0.81	22.54	12.98
Component C3	C	1737	119.17	97.30	0.82	22.25	12.80

Table 4: Crashworthiness parameters for an AA6063-T5 circular extrusion and for the proposed design obtained from quasi-static compression tests (both triggered) for a crushing distance of 228 mm. Collapse modes: C (concertina), D3 (3-lobe diamond).

4.3. Dynamic impact tests

The force-displacement curves obtained from the dynamic tests in the pendulum accelerator are shown in Figure 13a, where the corresponding quasi-static curves are presented as well for comparative purposes. These dynamic curves have been filtered using a moving-average filter to remove part of the high-frequency signals caused by the stress waves traveling along the load cell. Note that, as explained in Section 3.2, these results are only valid up to a crushing distance of 185 mm due to the presence of two safety buffers. Folding lengths were increased in the dynamic tests, as can be appreciated

in Figure 13a, where the distance between consecutive folding peaks is shorter in the quasi-static curve than in the dynamic curves. Average force-displacement curves are also provided in Figure 13b, where it can be seen that larger folding lengths in the dynamic tests led to a certain reduction of the mean force and, thus, the absorbed energy.

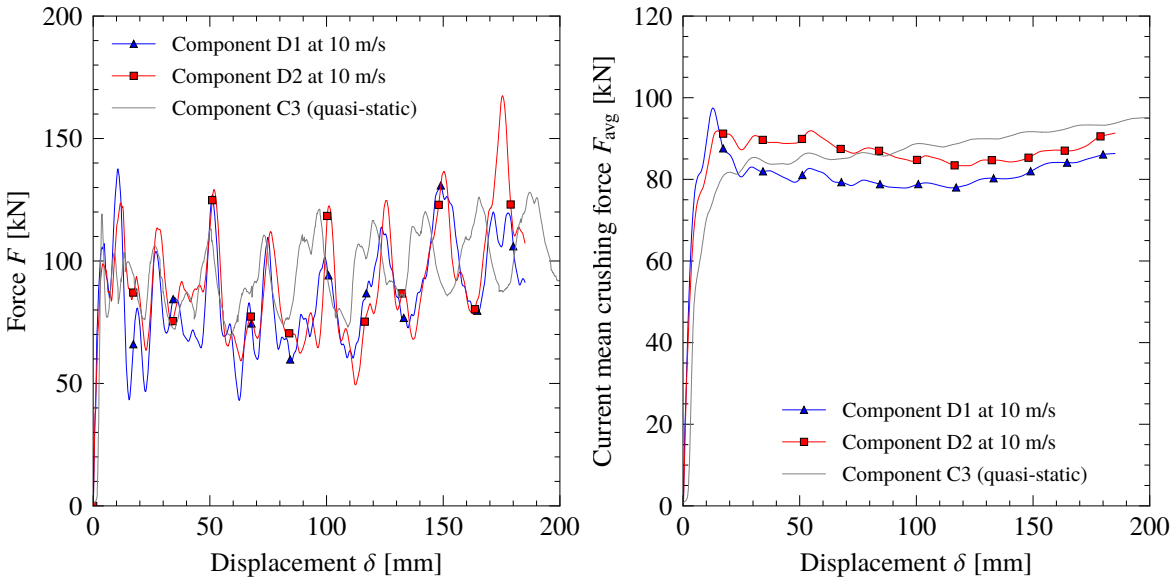

(a) Force-displacement curves.

(b) Average force-displacement curves.

Figure 13: Instantaneous and average force-displacement curves obtained from the dynamic impact tests on components D1 and D2 at 10 m/s. A slight reduction of the folding lengths can be observed in the dynamic curves compared to the quasi-static values.

Identical concertina collapse modes have been observed in both specimens (D1 and D2), matching those obtained for specimens C2 and C3. 18 folds were developed for a crushing distance of 225 mm, i.e. one less fold than the quasi-static specimens. A sequential view of one of the tests is offered in Figure 14, and a view of components D1 and D2 after impact is provided in Figure 15

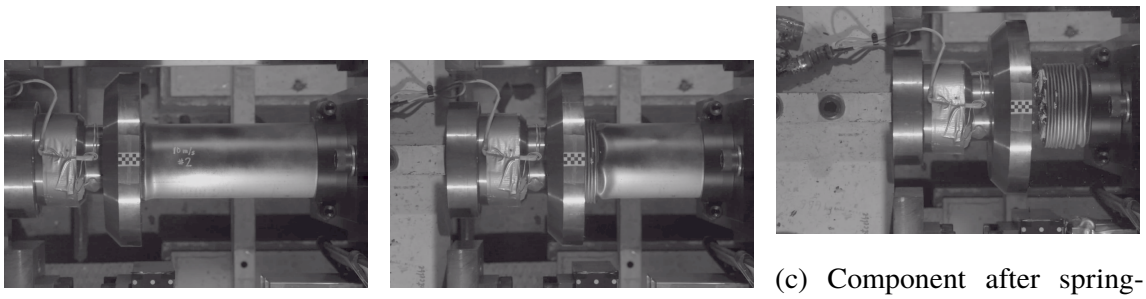

(a) δ = 5 mm, t = 0.51 ms.

(b) δ = 5 mm, t = 9.66 ms.

(c) Component after spring-back.

Figure 14: Sequential images from the 10 m/s impact test of component D2 in the kicking machine (top view).

Figure 15: Components D1 (left) and D2 (right) after impact test at 10 m/s. The clamped length of 50 mm is clearly appreciable.

The absorbed energy up to 185 mm of components D1, D2 and C3 is provided in Table 5. The slight decrease in energy absorption compared to the quasi-static tests was due to the reduction of the folding length observed in the dynamic components.

Component label	Absorbed energy up to 185 mm [kJ]
D1 (10 m/s)	15.92
D2 (10 m/s)	16.84
C3 (quasi-static)	17.31

Table 5: Energy absorbed up to an axial crushing of 185 mm by components D1 and D2 (impact) and C3 (quasi-static).

4.4. Assessment of the interaction effect of the polymeric foam

When foam-filled metal columns are subjected to a crushing process, it is usual to observe that the total force-displacement curve is higher than the sum of the curves corresponding to each part separately [12, 13]. This is due to the interaction of the foam with the metal walls: the foam acts as a constraint which reduces the buckling length and, therefore, increases the number of lobes to be developed. In the proposed design, this phenomena could appear between the foam and the extrusion and also between the foam

and the glass-fiber plates, since the former acts as a confinement which could contribute to a more efficient, progressive failure of the latter.

Hanssen et al. [12, 13] investigated the interaction between aluminum foam fillings and aluminum extrusions. In particular, they developed an additive design formula to obtain the average crushing force of circular aluminum extrusions with aluminum foam filler accounting for the interaction effect. This formula reads as

$$F_{\text{avg}} = F^0_{\text{avg}} + A_f \sigma_f + C_{\text{avg}} \sigma_f^{\alpha} \sigma_0^{(1-\alpha)} b_m^{\beta} h^{(2-\beta)}, \tag{8}$$

where F_{avg} is the total average crushing force, F^0_{avg} is the average crushing force of the empty aluminum extrusion, σ_f is the yield stress of the aluminum foam, b_i is the inner diameter of the extrusion, σ_0 is the yield stress of the aluminum alloy, $b_m = b - h$, and b and h are the outer diameter and wall thickness of the extrusion, respectively. Lastly, C_{avg}, α and β are parameters to be calibrated.

Since this design contains three different materials, it was necessary to evaluate each material separately in order to analyze how far the total response of the crash box was better than the sum of the three materials separately. However, neither the foam prisms nor the glass-fiber structure can be crushed alone: the foam columns buckle outwards and the GFRP plates fall apart after incipient fracture. Therefore, both materials were analyzed inside the aluminum extrusion and denoted CG (GFRP) and CF (foam), Table 3.

The force-displacement curves for CG and CF specimens are plotted in Figure 16a, together with the curves obtained for the aluminum extrusion alone (C0) and the complete component C1. Specimen C1 was chosen because its mixed collapse mode is more similar to the ones obtained for specimens C0, CF and CG. It is clearly seen that the individual contribution of the foam and the glass fiber plates was very small (see Figure 16a), which is an indicator of the presence of some kind of additional contribution generated by the interaction between the materials.

It was analyzed if this phenomenon could be explained with the well-known interaction effect between the foam and the aluminum extrusion, even though the contacts between these parts are not closed before crushing. To this end, and following Hanssen's procedure [12, 13], the curves for the empty extrusion (C0), the foam-filled extrusion (CF), an estimation of the response of the foam prisms in uniaxial compression and the sum of this estimation and the empty extrusion were plotted together (see Figure 16c). The estimation was made because of the infeasibility of obtaining the crushing response of the foam prisms alone without buckling. In view of the curves, it can be seen that the sum of C0 and

foam is approximately equal to the response of specimen CF (see curves in Figure 16c and absorbed energies in Table 6), and therefore it can be stated that the interaction effect between foam and extrusion is negligible. However, an improvement of the interaction levels was observed as the crushing length increased, which was due to the fact that the space between foam and extrusion closed with the axial compression. Hence, closing the space between materials when designing a multi-material component for energy absorption is important.

Once the interaction between foam and extrusion was found to be of minor importance, the force-displacement curves of component C1 to the sum of specimen CG and the estimated response of the foam were compared (see Figure 16e). A major difference between these curves was now observed and gray-shaded. Given that the foam is negligibly interacting with the extrusion, this improvement can only be due to the interaction (or confinement) of the foam and the glass-fiber plates. Indeed, the foam constrains the plates so that they do not fell apart after their first brittle fractures and keeps them in position for further degradation. In order to quantify this effect, the absorbed energies of component C1, CG and the sum of CG and foam are provided also in Table 6. A major difference (from 16.76 kJ to 23.57 kJ) arises as a consequence of the interaction effect.

	C0	CG	CF	Foam (est.)	C0 + foam	CG + foam	C1
E_a at $\delta = 228$ mm [kJ]	12.30	14.04	16.08	2.72	15.02	16.76	23.57

Table 6: Energy absorbed by the compared specimens up to 228 mm.

With the aim of verifying this last statement, component C3 was cut (see Figure 12e) and compared the extracted GFRP debris with the spare GFRP fragments resulting from specimen CG. A comparison of the sizes of the fragments showed that the GFRP was more severely damaged when confined by the foam, Figure 17, and thus an increased contribution to the global energy absorption was achieved.

In order to quantify this interaction, and based on [12], α and β are taken equal to 0.5 and 1, respectively, for Equation (8). The value of σ_f was taken equal to $\sigma_{0.3} = 933.27$ kPa and $A_f = 9475.37$ mm^2, $\sigma_{0.3}$ being the compression true stress corresponding to a true strain of 0.3 at a rate of 6 mm/min. This value has been taken as representative for the stress plateau in the stress-strain response of the foam. Due to the presence of mixed

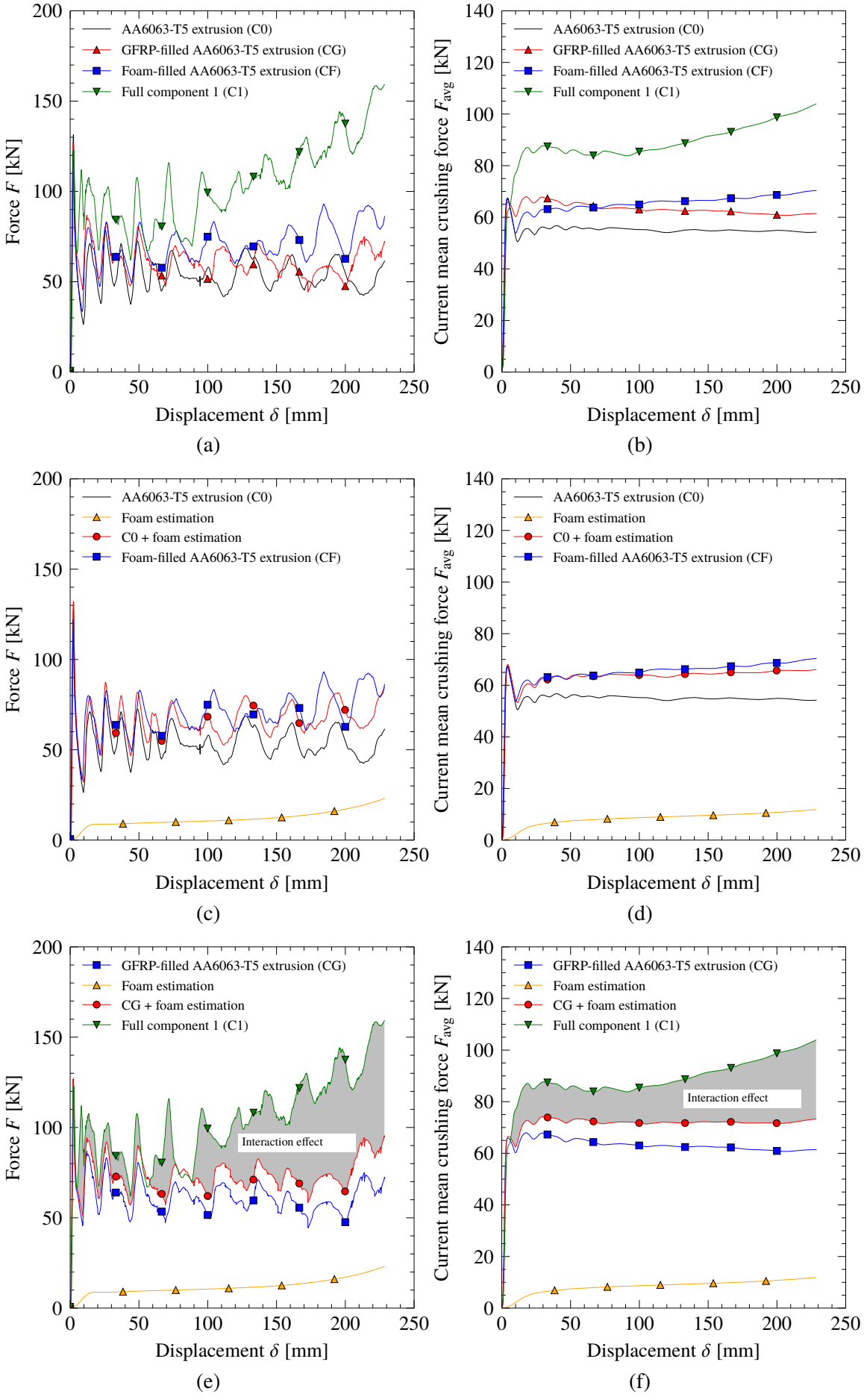

Figure 16: Force-displacement curves of different material combinations for the evaluation of the interaction effects in the proposed design.

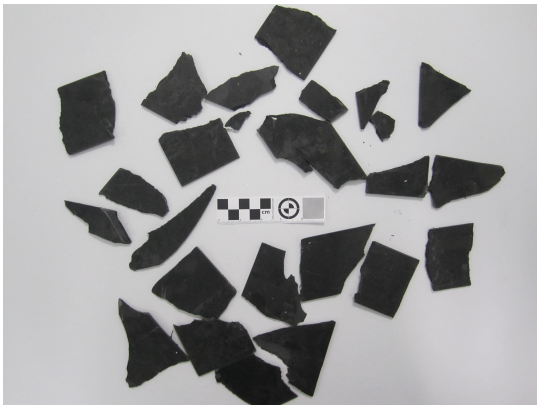

(a) GFRP debris after crushing specimen CG

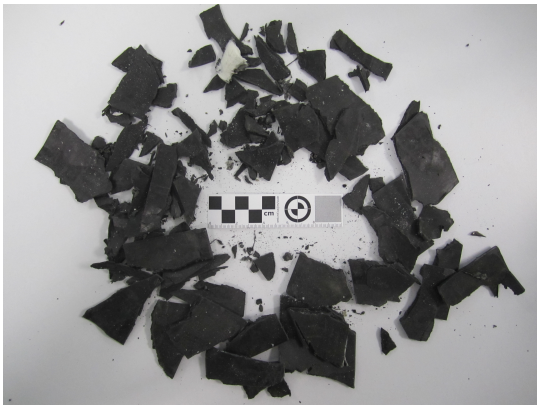

(b) GFRP debris after crushing component C3

Figure 17: Comparison of the fragments of GFRP after crushing of specimen CG and component C3. A more important degradation is observed for the latter.

collapse modes, the average crushing force of the empty aluminum extrusion is obtained from the experiments, with a value of 53.84 kN. Furthermore, the last term of Hanssen's original equation was modified in order to account for the mechanical properties of the GFRP. To that end, the ultimate tensile strength $\sigma_u = 200\,\text{MPa}$ has been included. The exponents of this last term were changed to $1/3$ to keep the dimensional consistency of the formula. To sum up, the expression proposed for our design reads as

$$F_{\text{avg}} = F^0_{\text{avg}} + \sigma_f A_f + C_{\text{avg}} \sqrt[3]{\sigma_f \sigma_0 \sigma_u} b_m h \tag{9}$$

The GFRP sheets cannot be crushed without a confinement because they buckle and fall apart. Therefore, their contribution is linked to the interaction effect. For this reason, the first addend (F^0_{avg}) refers to the average crushing force of the aluminum tube, i.e., the full component without any filling. This is related to the term in Hanssen's equation for the empty extrusion F^0_{avg}, which also corresponds to the full component minus the foam part. The values of C_{avg} were obtained for different crushing lengths and compared to the values obtained by Hanssen. These values are presented in Table 7.

Crushing length (%)	20	30	40	50	60
C_{avg} (Hanssen) [13]	1.08	2.07	2.45	2.74	2.90
C_{avg} (present)	2.46	2.65	3.09	3.67	4.29

Table 7: C_{avg} parameters for circular extrusions filled with aluminum foam (Hanssen, [13]) and circular extrusions filled with PET foam and GFRP (present).

In view of Table 7, it can be stated that the interaction effect for the proposed design linked to the term $C_{\text{avg}}\sqrt[3]{\sigma_f \sigma_0 \sigma_u} b_m h$ was larger than for Hanssen's design, but in the same order of magnitude. This increment was due to the strong interaction between foam and GFRP and also to the fact that the contribution of the GFRP alone was negligible, i.e. its contribution arose only from its interaction with surrounding materials.

5. Conclusions

An experimental study on the crashworthiness of a three-material crash box has been carried out, including a material testing campaign. The components were analyzed quasi-statically and under impact and the following conclusions can be drawn:

- It was observed that aluminum alloy AA6063 in temper T5 exhibits a very good performance in energy absorption by axial crushing, due to its high yield stresses and sufficient ductility. Only minor fracture initiations were found.

- The energy absorption of the aluminum tube reinforced with PET foam and GFRP increased by almost 100% when compared to an empty extrusion, in exchange for a 16% reduction of the specific energy absorption. Besides, the crush force efficiency was increased from 0.41 to 0.83. The components behaved in a very similar way at quasi-static and dynamic loading conditions.

- The separate contributions of the three different materials to the force response of the complete component were analyzed and quantified, as well as the interaction and confinement effects. A strong contribution was found in the interaction between the glass fiber and the foam, since the latter confined the former enhancing its performance. Moreover, a negligible interaction was observed between the foam and the extrusion. This is due to the fact that both parts are not in closed contact in the undeformed configuration. Finally, the interaction effects in the proposed design arising from the foam-GFRP interface have been quantitatively compared to the ones observed for aluminum foam filled extrusions.

- The quantification of the interaction effect was carried out using a modification of Hanssen's formula for foam-filled sections. This modification consisted of including the ultimate tensile strength of the glass fiber in the interaction term, with the correspondent change of exponents for dimensional consistency.

- The absorbed energy of the aluminum extrusions reinforced only with PET foam or only with GFRP was not significantly higher than the absorbed energy of the empty extrusion, given the excellent characteristics of the alloy; but a very remarkable enhancement was indeed produced when all the three materials were combined in a single design. This is explained by the fact that the foam confines the glass fiber plates, improving their performance.

Acknowledgments

The research leading to these results has received funding from the Galician Regional Government (Xunta de Galicia) under the plan GRC2013-056 and from foundations Fundación Barrié and CEAGA. The authors fully acknowledge the support received. The authors also want to thank engineers Tore Wisth and Trond Auestad for their essential collaboration and their excellent job preparing the laboratory specimens and equipments, respectively. Finally, we are grateful to H. Chapelle (Armacell) for kindly providing the PET foam required in this study.

References

[1] A. Reyes, O. Hopperstad, A. Hanssen, M. Langseth, Modeling of material failure in foam-based components, International Journal of Impact Engineering 30 (2004) 805 – 834.

[2] H. Yin, Y. Xiao, G. Wen, Q. Qing, Y. Deng, Multiobjective optimization for foam-filled multi-cell thin-walled structures under lateral impact, Thin-Walled Structures 94 (2015) 1 – 12.

[3] J. M. Alexander, An approximate analysis of the collapse of thin cylindrical shells under axial loading, Quarterly Journal of Mechanics and Applied Mathematics 13 (1960) 10–15.

[4] T. Wierzbicki, W. Abramowicz, On the crushing mechanics of thin-walled structures, Journal of Applied Mechanics, Transactions ASME 50 (1983) 727–734.

[5] T. Wierzbicki, S. Bhat, W. Abramowicz, D. Brodkin, Alexander revisited—a two folding elements model of progressive crushing of tubes, International Journal of Solids and Structures 29 (1992) 3269 – 3288.

[6] W. Abramowicz, T. Wierzbicki, Axial crushing of multicorner sheet metal columns, Journal of Applied Mechanics, Transactions ASME 56 (1989) 113–120.

[7] W. Abramowicz, N. Jones, Dynamic progressive buckling of circular and square tubes, International Journal of Impact Engineering 4 (1986) 243–270.

[8] A. Pugsley, On the crumpling of thin tubular struts, Quarterly Journal of Mechanics and Applied Mathematics 32 (1979) 1–7.

[9] A. Singace, H. Elsobky, Further experimental investigation on the eccentricity factor in the progressive crushing of tubes, International Journal of Solids and Structures 33 (1996) 3517–3538.

[10] S. R. Reid, T. Y. Reddy, Axial crushing of foam-filled tapered sheet metal tubes, International Journal of Mechanical Sciences 28 (1986) 643–656.

[11] S. R. Reid, T. Y. Reddy, M. D. Gray, Static and dynamic axial crushing of foam-filled sheet metal tubes, International Journal of Mechanical Sciences 28 (1986) 295–322.

[12] A. Hanssen, M. Langseth, O. Hopperstad, Static and dynamic crushing of square aluminium extrusions with aluminium foam filler, International Journal of Impact Engineering 24 (2000) 347 – 383.

[13] A. Hanssen, M. Langseth, O. Hopperstad, Static and dynamic crushing of circular aluminium extrusions with aluminium foam filler, International Journal of Impact Engineering 24 (2000) 475 – 507.

[14] S. P. Santosa, T. Wierzbicki, A. G. Hanssen, M. Langseth, Experimental and numerical studies of foam-filled sections, International Journal of Impact Engineering 24 (2000) 509–534.

[15] M. Seitzberger, F. Rammerstorfer, R. Gradinger, H. Degischer, M. Blaimschein, C. Walch, Experimental studies on the quasi-static axial crushing of steel columns filled with aluminium foam, International Journal of Solids and Structures 37 (2000) 4125–4147.

[16] A. Reyes, O. Hopperstad, M. Langseth, Aluminum foam-filled extrusions subjected to oblique loading: experimental and numerical study, International Journal of Solids and Structures 41 (2004) 1645 – 1675.

[17] S. Ouellet, D. Cronin, M. Worswick, Compressive response of polymeric foams under quasi-static, medium and high strain rate conditions, Polymer Testing 25 (2006) 731 – 743.

[18] U. K. Chakravarty, An investigation on the dynamic response of polymeric, metallic, and biomaterial foams, Composite Structures 92 (2010) 2339 – 2344.

[19] I. M. Daniel, J.-M. Cho, B. T. Werner, Characterization and modeling of stain-rate-dependent behavior of polymeric foams, Composites Part A: Applied Science and Manufacturing 45 (2013) 70 – 78.

[20] J. Liu, D. Saletti, S. Pattofatto, H. Zhao, Impact testing of polymeric foam using hopkinson bars and digital image analysis, Polymer Testing 36 (2014) 101 – 109.

[21] A. Mamalis, D. Manolakos, M. Ioannidis, D. Chronopoulos, P. Kostazos, On the crashworthiness of composite rectangular thin-walled tubes internally reinforced with aluminium or polymeric foams: Experimental and numerical simulation, Composite Structures 89 (2009) 416 – 423.

[22] A. Othman, S. Abdullah, A. Ariffin, N. Mohamed, Investigating the quasi-static axial crushing behavior of polymeric foam-filled composite pultrusion square tubes, Materials and Design 63 (2014) 446 – 459.

[23] M. Costas, J. Díaz, L. Romera, S. Hernández, A. Tielas, Static and dynamic axial crushing analysis of car frontal impact hybrid absorbers, International Journal of Impact Engineering 62 (2013) 166–181.

[24] E. H. Hanefi, T. Wierzbicki, Axial resistance and energy absorption of externally reinforced metal tubes, Composites: Part B 27B (1996) 387–394.

[25] H.-W. Song, Z.-M. Wan, Z.-M. Xie, X.-W. Du, Axial impact behavior and energy absorption efficiency of composite wrapped metal tubes, International Journal of Impact Engineering 24 (2000) 385–401.

[26] J. Starbuck, G. Jacob, D. Dillard, D. Pohlit, Crashworthiness of adhesively bonded composite structures and their strain-rate sensitivities, in: Proceedings of the 2006 SEM Annual Conference and Exposition on Experimental and Applied Mechanics 2006, volume 4, 2006, pp. 1808–1819.

[27] M. Bambach, M. Elchalakani, X. Zhao, Composite steel-cfrp shs tubes under axial impact, Composite Structures 87 (2009) 282–292.

[28] K. Shin, J. Lee, K. Kim, M. Song, J. Huh, Axial crush and bending collapse of an aluminum/GFRP hybrid square tube and its energy absorption capability, Composite Structures 57 (2002) 279–287.

[29] M. Stamenović, S. Putić, M. Zrilić, J. Milović, L.J.and Pavlović-Krstić, Specific energy absorption capacity of glass-polyester composite tubes under static compressive loading, Metalurgija 50 (2011) 197–200.

[30] M. Costas, J. Díaz, L. Romera, S. Hernández, A multi-objective surrogate-based optimization of the crashworthiness of a hybrid impact absorber, International Journal of Mechanical Sciences 88 (2014) 46–54.

[31] J. Paz, J. Díaz, L. Romera, M. Costas, Crushing analysis and multi-objective crashworthiness optimization of GFRP honeycomb-filled energy absorption devices, Finite Elements in Analysis and Design 91 (2014) 30 – 39.

[32] H. Zhu, L. Zhu, J. Chen, Damage and fracture mechanism of 6063 aluminum alloy under three kinds of stress states, Rare Metals 27 (2008) 64 – 69.

[33] V. Vilamosa, Behaviour and Modelling of AA6xxx Aluminum Alloys Under a Wide Range of Temperatures and Strain Rates, Ph.D. thesis, SIMLab (Structural Impact Laboratory), NTNU, 2015.

[34] BASF, Ultramid (r) A3WG10 BK00564 Polyamide 66. Product information sheet, 2015.

[35] ISO, Rigid cellular plastics – Determination of compression properties, ISO 844:2014, International Organization for Standardization, Geneva, Switzerland, 2014.

[36] A. Hanssen, T. Auestad, T. Tryland, M. Langseth, The kicking machine: A device for impact testing of structural components, International Journal of Crashworthiness 8 (2003) 385–392.

[37] M. Kristoffersen, Impact against X65 offshore pipelines, Ph.D. thesis, SIMLab (Structural Impact Laboratory), NTNU, 2014.